

Highly Sensitive Electrochemical Biosensor Based on Hairy Particles with Controllable High Enzyme Loading and Activity

Pavel Milkin, Anila Antony, Hongtao Cai, Antonia Debevc, Ceyda Topal, Anne Linhardt, Alla Synytska,* and Leonid Ionov*

For the first time, a highly sensitive electrochemical biosensor based on SiO₂ hairy particles grafted with polymerize poly(2-(dimethylamino)ethyl methacrylate) (PDMAEMA) polymer brushes containing immobilized *Laccase* from *Trametes versicolor* (TvL) is reported. This system offers major advantages in enzyme loading, catalytic efficiency, and detection sensitivity. The biosensor achieves a high enzyme immobilization density of up to 0.57 g g⁻¹ of polymer, while the enzymatic activity of the immobilized *Laccase* is enhanced 75-fold compared to the free enzyme in the buffer. These carriers are easy to handle and store, enabling reproducible sensor fabrication with well-defined enzyme content. The biosensor is tested for hydroquinone (HQ) detection, where *Laccase* rapidly catalyzes HQ oxidation near the electrode, generating a locally high quinone concentration. This suppresses direct HQ oxidation at the electrode surface, enhancing selectivity. The sensor demonstrates excellent analytical performance, with a sensitivity of 0.14 A·M⁻¹, a detection limit of 0.1 μM, and a wide linear range of 0.3–750 μM—surpassing most comparable systems even without optimization. This work serves as a proof of concept and a promising platform for developing advanced biosensors. Furthermore, the approach can be adapted to other core–shell particle systems and enzyme-based electrochemical detection platforms.

1. Introduction

Enzymes are increasingly used in biosensing applications due to their ability to accurately detect and quantify specific analytes.^[1] They function as bioreceptors, providing high selectivity and sensitivity to target molecules. Enzyme-based electrochemical biosensors offer several advantages, including high selectivity, rapid response times, ease of use, testing of nontransparent solutions, and potential for miniaturization, making them suitable for portable and cost-effective devices. These features have led to their widespread use in various fields, such as healthcare for disease diagnosis and monitoring,^[2] environmental monitoring for pollutant detection,^[3] and other industrial and research applications. However, limitations of many biosensors are i) low immobilization density, ii) difficulty of quantification of the amount of immobilized enzyme as well as iii) deactivation or denaturation of the enzyme during electrode fabrication, storage, or use,^[4] which can reduce enzyme activity, stability, and sensitivity over time.^[5]

Immobilizing enzymes on a suitable matrix can enhance their stability, reusability, and recovery as well as make their fabrication easier, which is crucial for improving biosensor performance.^[6] Techniques for enzyme immobilization include encapsulation, covalent bonding, physical adsorption, embedding, and chemical cross-linking, applied to systems like polymeric nanogels, hydrogels, or nanocomposites.^[7] In enzyme-based electrode development, enzymes are typically immobilized on electrode surfaces that have been modified with conductive and supportive materials. For example, *Laccase* from *Trametes versicolor* (belongs to the blue multicopper oxidases), which is considered in this work and able to oxidize phenolic compounds,^[8] was combined with multiwalled carbon nanotubes (MWCNT) to detect bisphenol A.^[9] Moreover, it was combined with graphene,^[1a] gold nanoparticles/MoS₂,^[10] gold/MXenes^[11] to detect catechol and other compounds. The direct immobilization of enzymes on the sensor surface by drop-casting or adsorption is not very technologically promising because i) the density of the enzyme is small; ii) the binding of the enzyme is weak and it can be washed off

P. Milkin, A. Debevc, C. Topal, L. Ionov
Faculty of Engineering Sciences
University of Bayreuth
Ludwig Thoma Str. 36A, 95447 Bayreuth, Germany
E-mail: leonid.ionov@uni-bayreuth.de

A. Antony, H. Cai, A. Linhardt, A. Synytska
Functional Polymer Interfaces Group
Bayerisches Polymerinstitut (BPI)
Universität Bayreuth
Universitätsstraße 30, 95447 Bayreuth, Germany
E-mail: alla.synytska@uni-bayreuth.de

 The ORCID identification number(s) for the author(s) of this article can be found under <https://doi.org/10.1002/adfm.202507589>

© 2025 The Author(s). Advanced Functional Materials published by Wiley-VCH GmbH. This is an open access article under the terms of the [Creative Commons Attribution](https://creativecommons.org/licenses/by/4.0/) License, which permits use, distribution and reproduction in any medium, provided the original work is properly cited.

DOI: 10.1002/adfm.202507589

during the measurement process; iii) the amount of immobilized enzyme is difficult to quantify. One way to i) increase the amount of immobilized enzyme and ii) make it's binding strong is to use polymer brushes – at certain conformation of polymer chains and grafting density on a surface. Enzyme molecules can penetrate between polymer chains which considerably increases loading capacity.^[12] Moreover, enzymes form multiple contacts with many polymer chains that ensure the stability of binding even if it is provided by weak bonds such as van der Waals interactions.

The use of carriers with already pre-immobilized active enzymes may ease the fabrication process of a sensor with any desired electrode when proper adhesion is possible. In addition, this fabrication process allows controlling the amount of immobilized enzyme because the amount of enzyme on the particles can be quantified, which cannot be achieved by directly depositing the enzyme on the substrate. As a model system, silica submicron particles are a suitable material due to the abundance of the -OH surface group, which can be easily used for different chemical modifications. The silica particles were already used in literature for enzyme immobilization. For instance, Bebic et al. used aminopropyltrimethylsilane (APTMS) to functionalize silica particles with amino groups for more stable electrostatic interaction with nucleophilic groups of enzyme.^[13] Our group went further and used (3-aminopropyl)triethoxysilane (APTES) modified silica carriers to polymerize poly(2-(dimethylamino)ethyl methacrylate) (PDMAEMA) brushes, which are polycation, physically adsorbing enzymes even more effective due to large charge density electrostatic interactions.^[14]

The use of carriers with an immobilized polymer brush layer (a combination of brush and carrier strategies) may allow i) considerably higher density of enzyme, ii) stability of its immobilization, and iii) reliable quantification of its amount. In fact, enzyme may be immobilized not only on the surface of the brush but inside of it and the amount of enzyme inside the brush may even exceed the amount of polymer forming brush. Moreover, the combination of the use of carrier and polymer brushes allows the combining of simplicity of despotising of enzyme and its high density. Particles loaded with enzymes were used for signal amplification of immune sensors.^[15] In this particular work, the *Laccase from Trametes versicolor* was used to amplify the analyte binding signals to the detection side, rather than detecting the analyte itself – this requires an additional step involving adsorption/washing of particles with immobilized enzyme, which also requires appropriate calibration.

In our work, we demonstrate, for the first time, the fabrication of a high-sensitivity enzymatic electrochemical biosensor using solid particles with a grafted polymer brush and a quantified amount of immobilized enzyme. We demonstrate this principle in the example of the physical immobilization of laccase in PDMAEMA brushes grafted onto submicron silica particles for electrochemical biosensing of hydroquinone in aqueous solutions. This system serves as a model, illustrating the potential of using PDMAEMA-decorated nano- and submicron particles to carry enzymes for bioelectrocatalysis. These carriers offer the advantage of quantitatively controlling enzyme immobilization via physical adsorption in brushes and can be stored as a suspension in buffer before being cast onto an electrode. The immobilized laccase efficiently oxidized hydroquinone, diminish-

ing hydroquinone oxidation process on the electrode's active surface and significantly amplifying the reduction current that allows higher sensitivity of biosensors. In this paper, we disclose the mechanisms of such biosensor.

2. Results and Discussion

2.1. Synthesis of Carrier Materials and Enzyme Immobilization

Initially, SiO₂ submicron particles were synthesized through the hydrolysis of tetraethyl orthosilicate (TEOS), with detailed synthesis steps outlined in previous studies.^[14] The general synthetic process for hairy SiO₂-PDMAEMA particles is illustrated in **Figure 1**. First, SiO₂ particles were modified using aminopropyltriethoxysilane (APTES) to introduce a significant number of amino groups on their surface. Subsequently, these amino groups were converted into bromine-containing groups through a reaction with a bromine initiator. Finally, surface-initiated Atom Transfer Radical Polymerization (SI-ATRP) was employed to graft PDMAEMA brushes onto the surface. The morphology and microstructure of SiO₂-PDMAEMA were characterized using electron microscopy. As depicted in **Figure 2a**, the uniform-in-size SiO₂ particles were synthesized, and after grafting PDMAEMA brushes, the polymer bridges became clearly visible, indicating successful polymerization. The diameters of the SiO₂ particles as measured by SEM were ≈230 nm, which increased to 250 nm after polymerization (**Figure 2b**). The particles exhibited a high degree of uniformity, as evidenced by their narrow size distribution.

We used thermogravimetric analysis (TGA) to accurately quantify the thickness of the polymer brush in the dry state (**Figure 2c**; **Figure S3**, Supporting Information). First, evaporation of adsorbed water occurs up to ≈ 200 °C. This point was considered as an initial mass for further calculations. Then, for native SiO₂ particles, there is a mass loss of about 10% at $T > 200$ °C which may be caused by the loss of bound water in the SiO₂ particles. After grafting, the mass loss at $T > 200$ °C was around 20% which was due to the incineration of PDMAEMA brushes. According to calculation with the Equation (8), the thickness of the polymer brush in the dry state is 5.22 nm. The value of grafting density obtained from the thickness of the brush and gel permeation chromatography (GPC) results were in the range of 0.23 chains·nm⁻² (**Table 1**).

The zeta potential instrument was utilized to assess changes in electro-kinetic potential across different pH levels. As illustrated in **Figure 2d**, the electro-kinetic potential of native SiO₂ particles remains consistently negative. Following modification with a bromine initiator, the isoelectric point of the particles shifts to pH = 5.2. After grafting with a PDMAEMA polymer brush, this point further shifts to pH = 9.6. This indicates that at pH = 4, which was utilized in this work, the particles exhibit a highly positive potential (≈40 mV) due to the protonation of tertiary amino groups. In previous work, it was shown, that this pH is optimal for high efficiency of enzyme immobilization.^[14] Such a positive electro-kinetic potential is advantageous for enzyme loading, as *Laccase* typically carries a negative charge in buffer solutions at pH = 4. This leads to the successful adsorption of enzyme to the polymer brushes via electrostatic interaction. Native, unmodified SiO₂ (used as a control) and SiO₂-PDMAEMA particles were

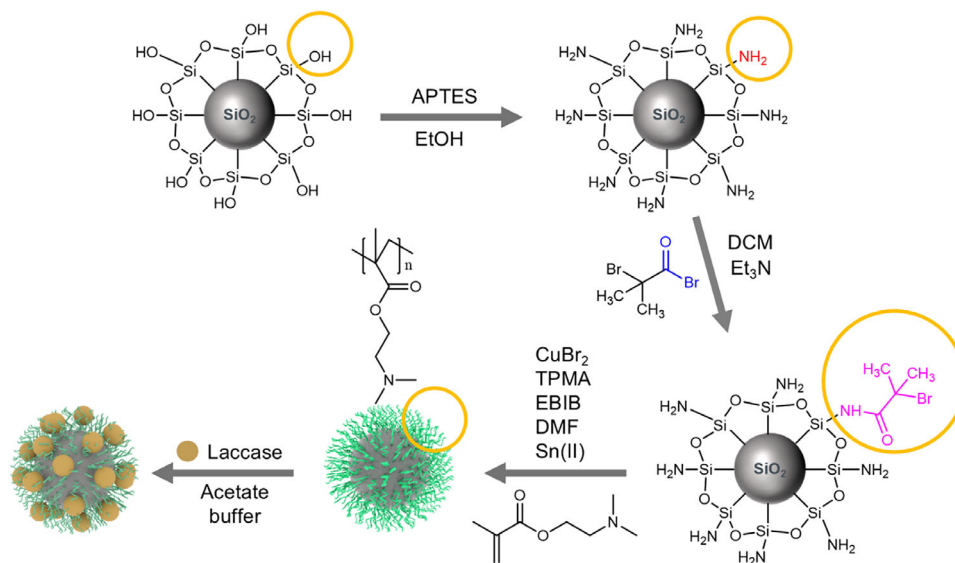


Figure 1. The scheme of surface modification of SiO₂ particles with APTES followed by surface-initiated ATRP of DMAEMA for brushing the particles and Laccase immobilization.

used for the immobilization of $\approx 16 \text{ U}\cdot\text{mL}^{-1}$ (or $0.32 \text{ U}\cdot\text{mg}^{-1}$ of enzyme) of initial enzyme activity under the same conditions. After immobilization, the activity of the enzyme on the particles was measured as ≈ 0.1 and $\approx 11 \text{ U}\cdot\text{mL}^{-1}$, respectively. The results show that enzymes are not immobilized on native SiO₂ particles without polymer brushes (Figure S1, Supporting Information). The activity of immobilized enzymes calculated per mg of particles, polymer, and enzymes are 1.13, 13.59, and $23.75 \text{ U}\cdot\text{mg}^{-1}$, respectively (Table 1). Thus, the final value is highly significant, demonstrating that the PDMAEMA brush environment provides favorable conditions for high enzyme immobilization density and enhanced activity, which is increased by 75 times ($0.32 \text{ U}\cdot\text{mg}^{-1}$ for pure enzyme to $23.75 \text{ U}\cdot\text{mg}^{-1}$ for enzyme in the brush) compared to the initial enzyme suspension in buffer. The increase in enzyme activity can occur for two reasons: i) the enzyme becomes truly active ii) the original enzyme contains an inactive impurity that is not immobilized on the particles, which increases the apparent activity. Within the current work, we cannot answer which hypothesis is correct.

TGA measurements revealed a considerable amount of enzymes embedded in the brush: 0.57 g of enzyme per 1 g of PDMAEMA at a dry brush thickness of 5.2 nm. The higher loading was observed only for the cellulase enzymogel adsorbed on SiO₂ particles grafted with polyacrylic acid brushes ($\approx 2 \text{ g}\cdot\text{g}^{-1}$ of polymer).^[12] If we assume that enzymes cover the outer layer of the polymer brush, then for the spherical hairy particles the enzyme layer thickness in the dry state is equal to 2.8 nm (at laccase density $1.37 \text{ g}\cdot\text{cm}^{-3}$).

Thus, hairy SiO₂ particles modified with PDMAEMA brush are capable of immobilizing a substantial amount of laccase and increasing its activity. By utilizing TGA and spectrophotometry, we can accurately determine the quantity of enzymes present in the particles and assess their activity. This allows for precise control over the amount and activity of enzymes immobilized on electrodes for electrochemical sensors. This level of precision was previously unattainable and is difficult to achieve with tradi-

tional enzyme immobilization methods like drop casting, commonly used by many researchers. Additionally, these enzyme carriers are easy to store and disperse, making them suitable for additive manufacturing of sensors, such as through inkjet printing.

2.2. Electrochemical Characterization of Electrodes

The electrochemical properties of bare and modified screen printed electrodes (SPEs) were assessed using cyclic voltammetry with the commonly used $[\text{Fe}(\text{CN})_6]^{3-}/4- \text{ redox couple}$ (Figure 3a). It is assumed that the transition between these two states is not catalyzed by laccase. As an analyte the 5 mM solution of $\text{K}_3[\text{Fe}(\text{CN})_6]$ in 0.1 M KCl was used – most of Fe in the solution is in oxidized form – Fe(III). The bare SPE exhibited broad and weak anodic and cathodic peaks with a large peak-to-peak separation value ($\Delta E = 0.89 \text{ V}$), significantly higher than the theoretical $\Delta E = 0.059 \text{ V}$, indicating quasi-reversibility of the process where reaction speed is not fast enough to maintain equilibrium during the scan and electrodes become polarized. Modification with nonconductive SiO₂ – PDMAEMA particles slightly decreased the peak-to-peak separation, but not significantly ($\Delta E = 0.77 \text{ V}$). Moreover, the shape of the waves becomes less symmetrical with a more pronounced cathodic peak. We attribute the asymmetry of the peaks in both cases to the diffusion limitation of the porous structure of screen-printed carbon electrodes. Due to the tortuosity of the porous structure, it takes more time for the analyte to reach electrode active sites. The introduction of charged PDMAEMA brushes leads to an even lower effective diffusion coefficient of the analyte.

Electrical impedance spectroscopy (EIS) of bare and modified SPEs in the same solution was conducted to investigate charge transfer behavior (Figure 3b; Figure S5, Supporting Information). Measurements were performed in the same solution at the formal potential of the redox couple with a 10 mV voltage

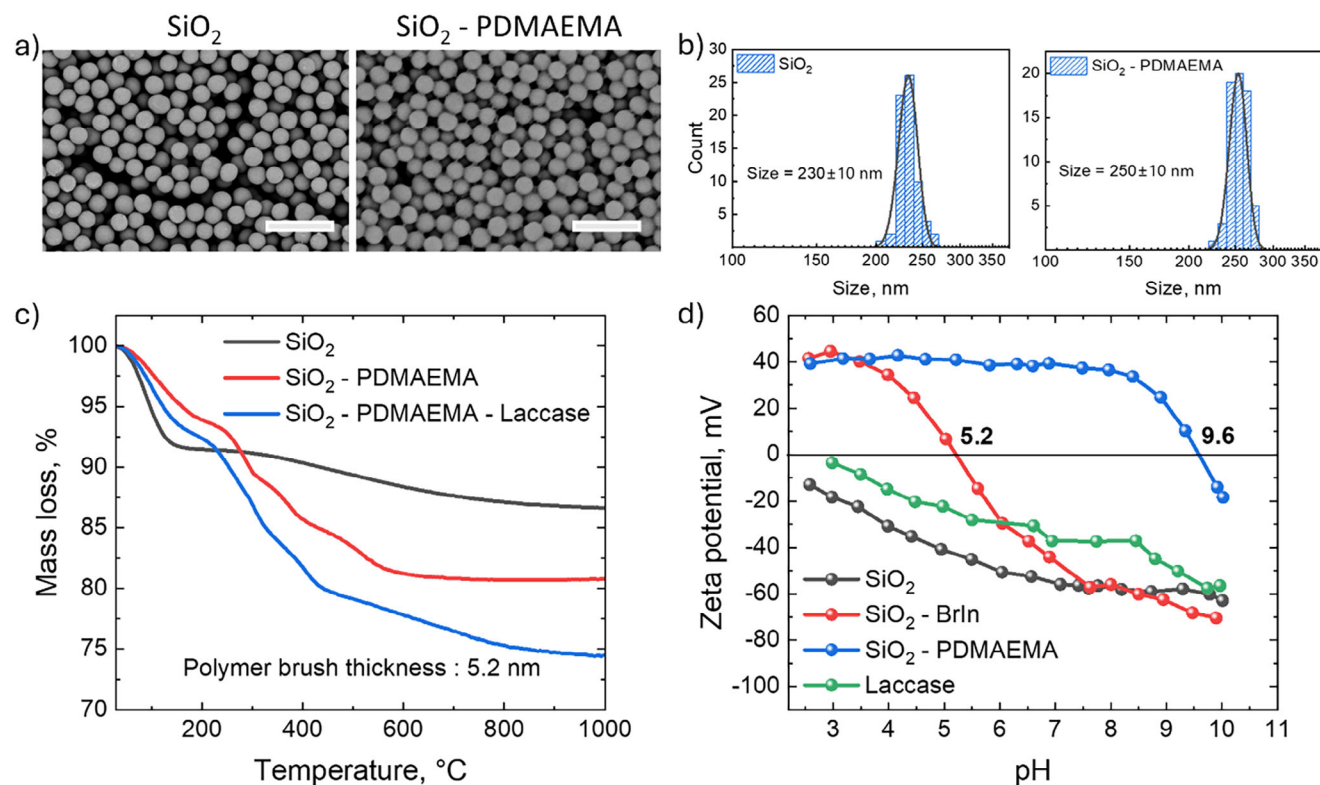


Figure 2. Properties of particles on different stages of synthesis: a) Representative SEM images of native SiO₂ and PDMAEMA brush-modified SiO₂ particles (scale bar is 1 μm) as well as (b) their size distribution function obtained from SEM images; c) TGA measurements of native, PDMAEMA brush modified SiO₂ particles, and hairy particles with immobilized laccase; d) Zeta-potential of SiO₂ particles after each stage of their surface modification as well as zeta-potential of Laccase as function of solution pH.

amplitude and 0 V offset. The results were fitted using a circuit model containing solution resistance (R_s) in series with one or two parallel R-CPE circuits. One R-CPE circuit corresponds to the charge transfer resistance (R_{ct}) and double-layer capacitance (CPE_{dl}). The second R_p - CPE_2 circuit we attribute to the charge transfer resistance and double-layer capacitance related to slower diffusive polycationic PDMAEMA brushes. The unmodified SPE electrode exhibited a higher charge transfer resistance (R_{ct}) of 14.9 kΩ compared to modified SPE by SiO₂ particles with brush and enzyme. Introducing nonconductive, brush-decorated particles reduced the R_{ct} by a factor of three to $R_{ct}^{SiO_2} = 4.7$ kΩ. This change can be attributed to the polyelectrolyte nature of the polymer brush, which locally increases ionic strength and decreases the Debye length ($\lambda_D \approx I^{-1/2}$, I – Ionic strength of electrolyte). The charge transfer rate constant was calculated according to Equation (6). Bare SPE possesses quite a low value of rate constant ($k_0 = 0.22 \cdot 10^{-3} \text{ cm} \cdot \text{s}^{-1}$). The addition of nonconductive SiO₂ particles results in a slight, but not significant increase in charge transfer rate constant ($k_0 =$

$0.27 \cdot 10^{-3} \text{ cm} \cdot \text{s}^{-1}$). Two semi-circles in the Nyquist plot for the SPE-SiO₂-PDMAEMA-Laccase sample can originate from inhomogeneity of electrode – part of carbon is not covered by particles and acts as a bare electrode. Thus, the surface modification by SiO₂ – PDMAEMA – Laccase particles does not significantly change the surface properties of the bare carbon working electrode.

2.3. Bioelectrocatalysis

Hydroquinone (HQ) was chosen as a substrate for the investigation of bioelectrocatalytic properties of SiO₂ – PDMAEMA – Laccase modified electrode. The oxidation of hydroquinone in air is a spontaneous process ($\Delta G_{298}^0 = -193.9 \text{ kJ} \cdot \text{mol}^{-1}$, the equilibrium constant for the reaction is high, $\approx K \approx 10^{33}$, Scheme S1, Supporting Information). The catalytic ability of laccase accelerates this reaction. The mechanism of hydroquinone detection is illustrated in Figure 4. Hydroquinone is catalytically oxidized by laccase immobilized in PDMAEMA brushes, forming

Table 1. Parameters of carriers modified by PDMAEMA brushes with immobilized laccase.

Brush thickness (TGA), nm	Grafting density, chain-nm ⁻²	Polymer M _n , kDa	Polymer M _w , kDa	Enzyme thickness (TGA), nm	Activity U·mg ⁻¹ of particles	Activity U·mg ⁻¹ of polymer	Activity U·mg ⁻¹ of enzyme
5.2	0.23	18.4	26.16	2.8	1.13	13.59	23.75

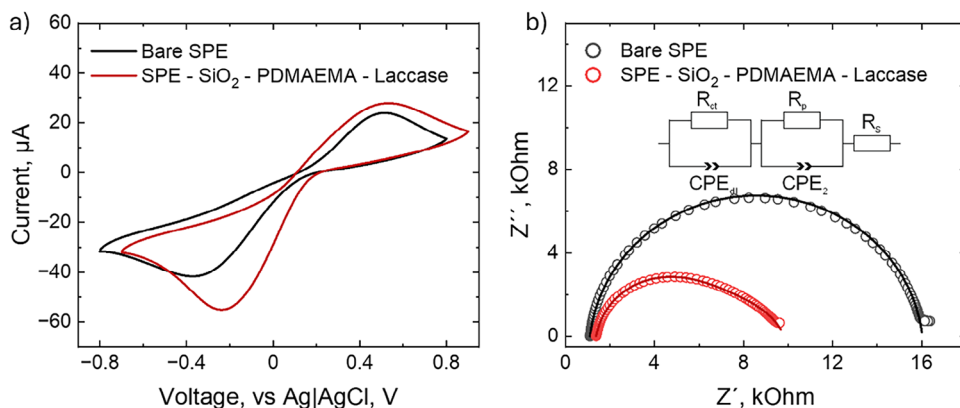


Figure 3. a) CV of SPE and SPE modified by SiO₂-PDMAEMA-Laccase particles electrodes, measured in a solution containing 5 mM K₃[Fe(CN)₆] and 0.1 M KCl; scan rate 50 mV·s⁻¹. b) EIS spectra of SPE and SPE modified electrodes obtained in the same solution at formal potential offset with 10 mV amplitude.

1,4-benzoquinone (Q) and the reduced form of laccase. The quinone is then electrochemically reduced at the working electrode, with the recorded current being proportional to the hydroquinone concentration in the solution. The reduced laccase is subsequently oxidized by molecular oxygen and remains unconsumed after the electrochemical reaction. Since the oxygen concentration in water at air (260 μM)^[17] is much higher than the Michaelis constant of laccase for oxygen (10 μM),^[17] and the laccase active center (copper) oxidation is a spontaneous process, the limiting step is the diffusion of quinone to the electrode surface. The reduction current value is used as the sensing signal.

To prove that Laccase catalyzes the reaction, we performed an electrochemical investigation of the HQ/Q redox process through cyclic voltammetry (CV) of four electrodes, modified with i) bare SiO₂ particles (SiO₂), ii) bare SiO₂ particles with immobilized on enzymes (SiO₂-laccase), iii) brush-decorated SiO₂ particles (SiO₂-PDMAEMA), and iv) brush decorated particles with immobilized laccase (SiO₂-PDMAEMA-laccase). To compare sensors between each other the current was normalized to the active surface area. The active surface area *A* was calculated based on CV results at different scan rates in 0.1 mM hydroquinone solution in 0.1 M pH = 4 acetate buffer (Figures S6 and S8, Supporting Information) using the Randles–Sevcik equation Equation (7). The taken values of *A* are illustrated in Table S2

(Supporting Information). The linear dependence of the cathodic peak on the square root of scan rate (Figure S7, Supporting Information) demonstrates the freely diffusing analyte. The peak shift with an increase in scan rate is observed. This means the electrochemical quasi-reversibility of the process.

All systems, except SiO₂ – PDMAEMA – Laccase demonstrate the symmetrical shape of the CV curve (Figure 5a) where anodic and cathodic processes occur quasi-reversibly only on the electrode surface and the cathodic peak value at -0.27 V is not significantly different and have value ≈50 μA·cm⁻² (Figure 5b). The symmetry of the CV curve means that the reaction is not catalytically amplified, i.e., the enzyme was not immobilized on native silica particles and products of catalytic reaction do not diffuse away from the electrode and remain in its vicinity. The significant increase in reduction signal and nearly disappearance of oxidation potential are observed for particles with laccase embedded in polymer brush with reduction peak value 136 μA·cm⁻² at -0.37 V. The larger overpotential value is due to the insulation effect of enzymes embedded in polymer brushes. It is worth noticing that amplification of the current was achieved even without signal normalization (Figure S6, Supporting Information), which is important for practical use: the current noise is lower, and the sensor can be miniaturized. Moreover, the current is higher compared to hairy particles without enzymes, meaning

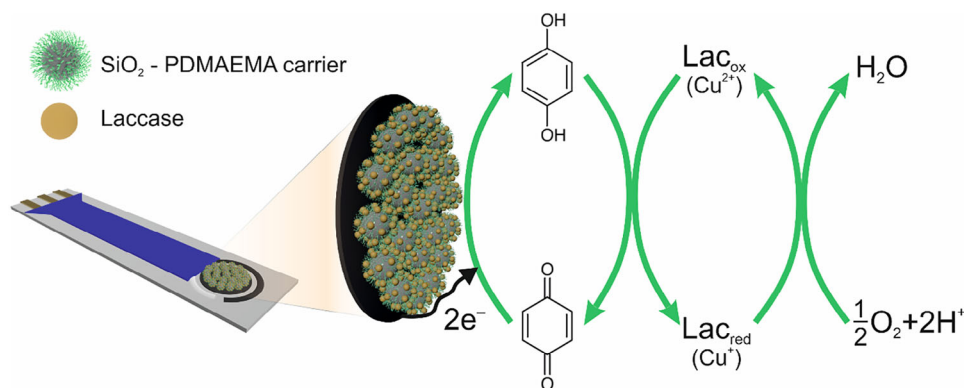


Figure 4. Schematic visualization of the redox process occurring on the laccase-carrier modified working electrode.

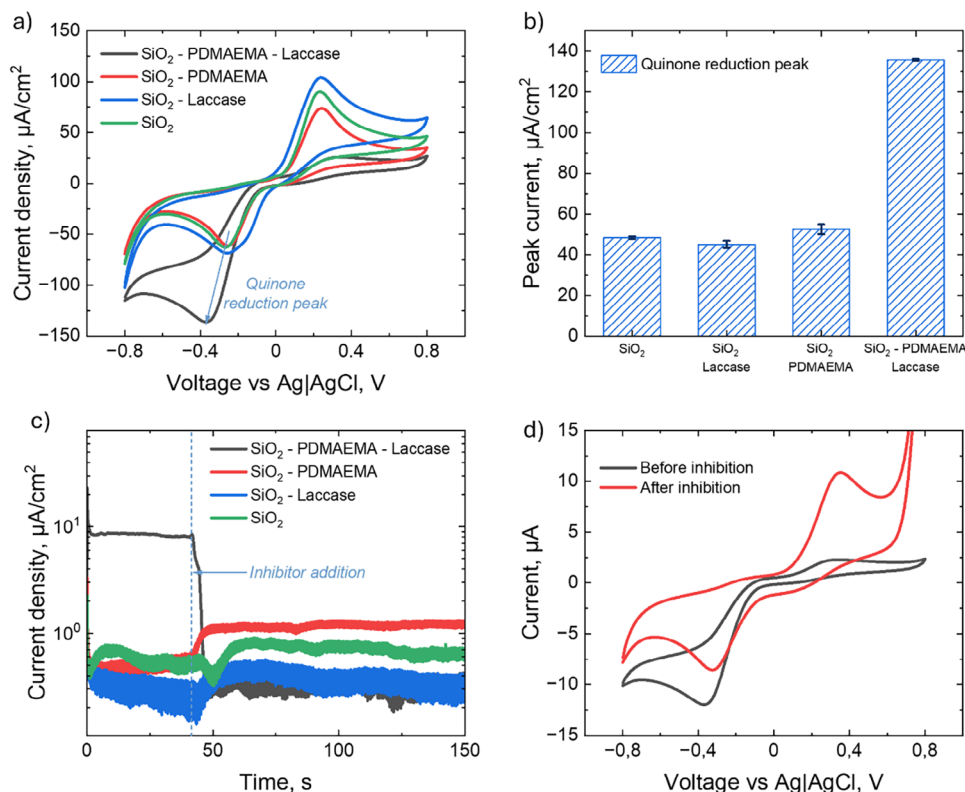


Figure 5. Electrochemical behavior of electrodes with different particles: a) CV of differently modified electrodes measured in 0.1 mM hydroquinone solution in 0.1 M pH = 4 acetate buffer at $100 \text{ mV}\cdot\text{s}^{-1}$; b) Quinone reduction peak values taken from CV results; c) chronoamperometry measurements at constant stirring with addition of NaN_3 solution as inhibitor; d) CV of SiO_2 -PDMAEMA-Laccase electrode before and after inhibition (measured at $100 \text{ mV}\cdot\text{s}^{-1}$).

a higher efficient concentration of Q near the surface than that of HQ in bulk. Thus, the addition of enzymes significantly diminishes the anodic peak and amplifies the cathodic one. The system starts to behave as a diode – conductivity is possible only in one direction (Figure S9, Supporting Information). The reason for that can be that enzymes oxidize hydroquinone (the process with negative free Gibbs energy) very fast and efficiently. The reduced quinone (hydroquinone) is very quickly oxidized by enzymes even in proximity to the electrode surface before oxidation potential is reached. As a result, contrary to the bulk of the solution which contains hydroquinone, there is only quinone near the electrode, which reduction is observed. Its oxidation happens on particles with immobilized enzymes.

To prove the impact of enzyme on signal amplification the enzyme inhibition test was performed (Figure 5c). The chronoamperometry was performed at $E = -0.6 \text{ V}$ versus the reference electrode at constant stirring to provide mass transfer of substrate to the electrode with addition of $100 \mu\text{L}$ of 0.1 M NaN_3 water solution as an inhibitor to the system. A significant drop in reduction current was observed for the SiO_2 -PDMAEMA-Laccase system due to hindrance of enzyme activity. For systems without laccase a slight increase of a current occurred due to a slight increase in ionic strength of the solution. CV curve made after inhibition (Figure 5d) in the same solution has a symmetrical shape, indirectly proving the diminishing of the anodic peak before inhi-

bition due to high enzyme activity. Thus, the PDMAEMA brush under this pH of solution and polymer chain conformation provides the conditions where activity of enzymes is elevated and the signal for hydroquinone sensing is significantly amplified.

To demonstrate that immobilizing enzymes on hairy particles before depositing them on an electrode is more advantageous than doing so afterward, we conducted CV measurements of electrodes (Figure S11, Supporting Information) modified with SiO_2 -PDMAEMA particles where enzymes were immobilized prior to particles deposition on the electrode, as previously used (SiO_2 -PDMAEMA-laccase). We compared the results obtained on the electrode modified with SiO_2 -PDMAEMA particles by first depositing empty hairy particles, followed by drop-casting a highly concentrated enzyme suspension (enzymogel). The absolute activity of enzymes used for immobilization was the same and equal to 0.15 U. SiO_2 -PDMAEMA particles without enzyme served as a reference. The results indicate a more significant amplification of the cathodic peak when laccase is immobilized into the brush beforehand (14.9 vs 10.6 μA). This suggests that the enzyme concentration is high, and their conformation allows for high catalytic activity. A disadvantage of the typical drop-casting method of enzymes on top of electrode, commonly used in other research projects, is that enzymes may be washed away due to poor adherence to the electrode, and their conformation may not be optimal for hydroquinone oxidation. Moreover, concentrated enzyme suspension acts as a gel and may hinder the substrate

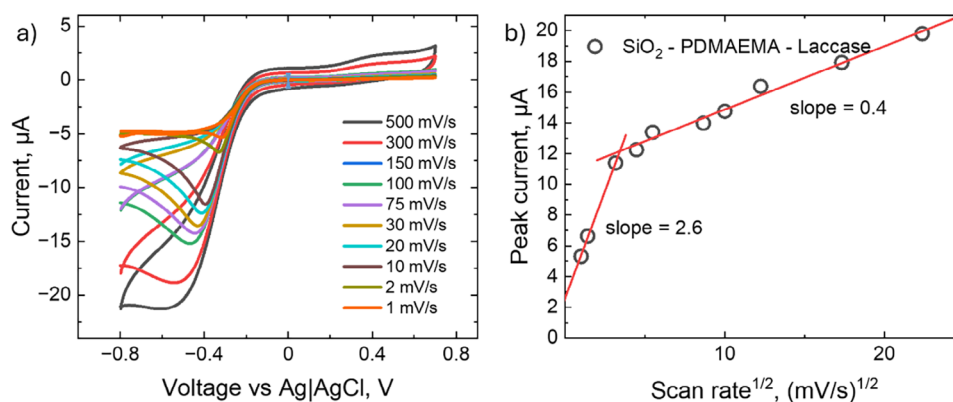


Figure 6. a) Cyclic voltammetry of SPE modified by SiO₂ – PDMAEMA – laccase particles measured at various scan rates in 0.1 mM hydroquinone solution in 0.1 M pH = 4 acetic buffer; b) cathodic peak current versus square root of scan rate obtained from cyclic voltammetry curves.

and mediator diffusion to the electrode surface. Thus, the use of hairy particles with immobilized enzymes provides advantages from both technological side (easy to calibrate and process) and from point of view of sensitivity.

The kinetic of hydroquinone detection exhibits distinct kinetic zones, observable in CV data for SiO₂–PDMAEMA–laccase modified electrodes across a wide range of scan rates (Figure 6a,b). In particular, a plot of the peak current versus the square root of the scan rate $v^{1/2}$ shows two different regimes with different slopes that reflect the diffusion coefficient, with a transition point at $\approx 12 \text{ mV}\cdot\text{s}^{-1}$.

The slope is steep at low scan rates and becomes shallower at high scan rates. We hypothesize that at high scan rates, quinone near the electrode is not significantly depleted, which suggests its effective transport to the electrode. The intercept of the linear dependence at high scan rates is $\approx 11 \mu\text{A}$, rather than 0. This nonzero current arises from the enzymatic conversion of hydroquinone to quinone, which follows Michaelis–Menten kinetics. Consequently, the peak current (i_p) dependence can be described by the following Equation (1):

$$i_p = \frac{i_{\max} \cdot [HQ]}{K_m + [HQ]} + K [Q] v^{1/2} \quad (1)$$

where $[HQ]$ – hydroquinone concentration, $[Q]$ – effective quinone concentration near electrode, i_{\max} – maximum current density at saturating substrate concentration at a given enzyme's concentration, K_m – Michaelis constant, K – proportionality coefficient of Randles–Sevcik equation. As the system approaches equilibrium, the positive scan reduction current stabilizes at a certain value. The transition point indicates the scan rate at which this equilibrium is reached.

At low scan rates, quinone near the electrode is significantly depleted. As a result, the limiting step in the process is likely its diffusion from the enzyme to the electrode surface, as well as the subsequent reduction of hydroquinone back to the enzyme (Figures S9 and S12, Supporting Information).

To explain observed behavior, we proposed the following model for low and high scan rates (Figures S12 and S13, Sup-

porting Information). Enzyme constantly catalyzes the oxidation of hydroquinone in the presence of dissolved oxygen independently of applied potential and scan rate. The rate of oxidation depends on the concentration of hydroquinone, which can diffuse to the enzyme from two sides: from the bulk of solution and from electrode if sufficient negative potential is applied for quinone reduction. Reducing applied potential from 0 down to -0.8 V results in beginning of the reduction of quinone diffused to electrode from the enzyme. The quinone is reduced when the potential below $\approx -0.3 \text{ V}$ and the current gradually decays that is due to consumption of quinone. It is reduced faster than new quinone is transported from the enzyme – the concentration of quinone close to the electrode drops as soon as the potential is lower than -0.3 V . The higher the scan rate, the shorter period the sufficiently negative potential ($\leftarrow 0.3 \text{ V}$) is applied to cause reduction of quinone and the smaller amount of quinone is consumed and the less pronounced is decay of current right after current peak was achieved. The lower is scan rate the lower the current because considerable quinone consumption. The lowest value of current at potential $\leftarrow 0.3 \text{ V}$ is $\approx 5 \text{ mA}$. This current corresponds to equilibrium between the rate of oxidation of hydroquinone to quinone by enzyme and the rate of reduction of quinone to hydroquinone at the electrode including also transport rates from electrode to enzyme and back. Applying positive potential, which must result in oxidation of hydroquinone, does not result in appearance of considerable current because hydroquinone is oxidized at the enzyme without charge transfer to the electrode – electrons are directly transferred to dissolved oxygen.

In order to prove that transport rates determine the shape of the CV curve, we performed catalyzed and non-catalyzed experiments with and without stirring. In a non-catalyzed system, CV without stirring looks symmetric: hydroquinone is oxidized to quinone, which stays in the vicinity of electrode and is reduced when a negative potential is applied. Stirring results in the disappearance of reduction peak because quinone is removed from the electrode (Figure S14a, Supporting Information). Applying stirring to the catalyzed system results in an increase in the reduction current and its slower decay because more hydroquinone is delivered to particles due to convection (Figure S14b, Supporting Information).

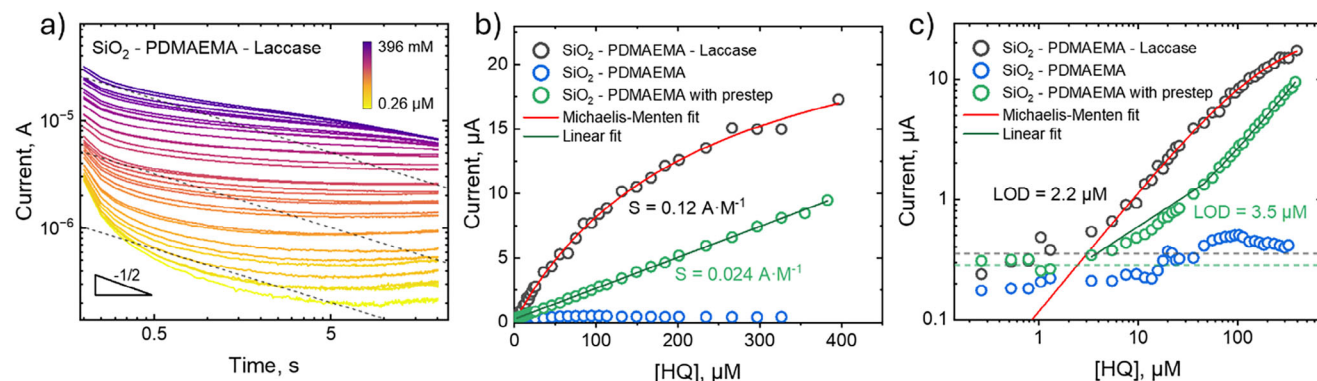


Figure 7. a) Chronoamperometry curves for SiO₂ – PDMAEMA – laccase modified SPE measured in solutions with various concentrations of hydroquinone at E = –0.6 V. Plotted in b) lin–lin and c) log–log coordinates calibration curves obtained from chronoamperometry measurements at t = 2 s for SiO₂ – PDMAEMA – laccase system and, as a control, for SiO₂ – PDMAEMA modified SPE without laccase, obtained at direct application of E = –0.6 V reduction potential (blue scatters) and with 30s prestep of E = 0.6 V (green scatters).

2.4. Sensor Parameters

For defining the sensor performance parameters, the calibration of the sensor was made by chronoamperometry measurements at E = –0.6 V (Figure 7a; Figure S15 and S17, Supporting Information) in acetate buffer with gradual addition of HQ solution. The current was plotted versus concentration at time t = 2s (Figure 7b,c) and t = 0.1s (Figure S18, Supporting Information). The main parameters such as lower and upper Limits of Detection (LOD), sensitivity (S), and detection range were assessed. The sensitivity was obtained from the slope of current versus concentration. The LOD is defined as a ratio of tripled standard deviation of background current to sensor sensitivity.

The current–concentration curve taken at t = 2s, at first glance, follows the Michaelis–Menten Equation (2) that is because the current reflects the rate of reaction:

$$i = \frac{i_{\max} \cdot [HQ]}{K_m + [HQ]} \quad (2)$$

where [HQ] – hydroquinone concentration, i_{\max} – maximum current density at saturating substrate concentration at a given enzyme's concentration, K_m – Michaelis constant. The sensitivity S, which is equal to $S = \frac{i_{\max}}{K_m}$, of SiO₂ – PDMAEMA – laccase modified SPE based sensor at t = 2 s was S = 0.12 A·M^{–1} what corresponds to the slope of current versus concentration dependences in linear region (Figure 7b). The Michaelis constant is equal to 0.23 mM which is relatively high compared to what can be found in the literature for this particular type of enzyme (< 0.1 mM).^[18] It means the low affinity of the enzyme to the substrate. The high affinity of enzymes usually leads to a lower upper detection limit of the sensor and experience signal off-scale. The large K_m provides the ability of sensor to detect large concentrations of hydroquinone at least up to 100 μM (in case of calibration at t = 2 s). That can be useful, for instance, for detection of hydroquinone in industrial effluents like polymers production, where hydroquinone is often used as an inhibitor of polymerization. The lower LOD was calculated as a tripled standard deviation of background cur-

rent without substrate divided by sensor sensitivity and equal to 2.2 μM.

However, a clear issue is observed: the calibration curve at t = 2 s tends to reach a plateau, whereas at t = 0.1 s, the plot remains mostly linear within the studied range of concentrations (Figure S18, Supporting Information). As we discussed previously, we assume that at low time scale there is HQ/Q diffusion (from electrode to enzyme and back) limitation, resulting in a plateau only at large concentrations of HQ: the reaction rate is fast and sensitive to Q concentration but negligible amount of the Q is consumed. However, at large time scale the enzymatic reaction is closer to equilibria state which results in a slower reaction rate and, as consequence, lower current dependency on mediator concentration. The Michaelis–Menten kinetics suggests that current saturation is due to the enzyme's catalytic capacity limitation. Then, the Michaelis constant should be independent of the chronoamperometric curve's time chosen for calibration, which is not the case here, indicating that the Michaelis–Menten model is not appropriate for this scenario. Therefore, both the saturation current as well as upper detection limit for the sensor cannot be truly estimated. Moreover, the correct comparison of our results to results of other researchers are also limited due to differences in detection mechanism (please, see the Supporting Information).

For reference, the calibration curve for SiO₂ – PDMAEMA particles modified SPE of the same carrier amount without laccase was obtained in the same concentration range (Figure 7b,c, green scatters). The results demonstrate the linear dependence of current on HQ concentration with sensitivity 5 times lower (S = 0.024 A·M^{–1}) than carriers with enzyme and with detection limit equal to 3.5 μM. The measurements were performed at the same E = –0.6 V with 30s prestep at E = 0.6 V for oxidation of hydroquinone at electrode proximity. Since the sensitivity is much lower and linearity is maintained even at large concentrations, it evidences the free diffusion of HQ to the active surface of the carbon electrode and the relatively low effective concentration of quinone. If the measurements were performed at constant voltage E = –0.6 V without oxidation prestep at E = 0.6 V, nearly no current was observed, which is expected in the absence of laccase.

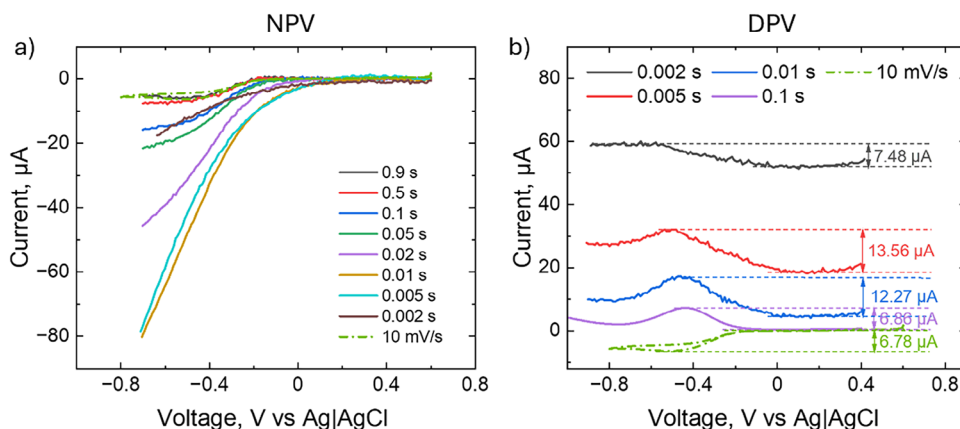


Figure 8. a) Normal pulse voltammetry (NPV) performed at 10 mV step varying pulse time normalized on a linear region curve where there is no faradaic current (raw data are shown in Figure S18 (Supporting Information)); b) Differential pulse voltammetry (DPV) performed at 10 mV step with 200 mV pulse amplitude and 1 s period varying pulse time. Measurements were performed for the SiO_2 – PDMAEMA – laccase sample in 0.1 mM HQ in 0.1 M pH = 4 acetate buffer. As a reference, a linear CV results at 10 mV s⁻¹ in the same solution is shown which corresponds to the same voltage scan rate.

Thus, the sensor based on SiO_2 -PDMAEMA-laccase particles contains an extremely high amount of enzymes, as current saturation is not due to the enzyme's catalytic capacity limit but rather the diffusion limitation of HQ/Q from electrode to laccase and back. The high enzyme activity within the PDMAEMA brushes and their abundance result in a large efficient concentration of quinone near the electrode surface, which provides a faster reaction at the electrode surface when reduction overpotential is applied. Providing mass transfer, incorporating convection, or using microelectrodes, could potentially extend the upper detection limit of the electrode even further, which is typically a limitation of enzyme-based sensors. Moreover, large absolute values of reduction current also allow the miniaturization of electrodes reducing the projecting surface area of electrode. Importantly, this approach can also be applied to other substrate-enzyme pairs when the conditions for immobilization and activity of another enzyme type are fulfilled.

2.5. Performance Optimization

To improve sensitivity and LOD, the current response should be increased and/or the current noise reduced. Two approaches can be used to achieve this: modifying the material or changing the measurement technique. In the first approach, we activated the graphite electrode in a NaOH solution to increase its active surface area and conductivity. Although this activation led to a higher current response and lower overpotential values (Figure S27, Supporting Information), it also resulted in an increased capacitive current and, consequently, higher noise. As a result, calibration of the sensor (Figures S28–S30, Supporting Information) with both activated and nonactivated surfaces showed no improvement in sensitivity ($S = 0.09 \text{ A} \cdot \text{M}^{-1}$ for both sensors). However, the LOD worsened significantly, increasing by a factor of 60 (4.5 vs 0.07 μM). Thus, while the conductivity increased, the sensor's overall performance—at least for graphite-based electrodes — did not improve.

As a second approach, for nonconductive SiO_2 carriers, higher registered currents can be achieved using alternative electro-

chemical methods. Normal pulse voltammetry (NPV) and differential pulse voltammetry (DPV) can enhance sensor sensitivity and lower the limit of detection (LOD). These methods facilitate the reduction of quinone at its high local concentrations on the electrode in a short time, where the reaction rate is high, thereby minimizing the impact of diffusion. Using NPV with short pulse times can increase the current by an order of magnitude (Figure 8a). Longer pulses result in a situation akin to a very low scan rate in linear CV, where HQ/Q diffusion reaches equilibrium, and the curve plateaus at cathodic overpotential (Figure S23, Supporting Information). A similar behavior is observed with DPV: shorter pulses lead to higher reaction rates and consequently increased current (Figure 8b). The peak current can be twice as high at a pulse time of 0.005 s compared to linear CV, although this is not the case for 0.002 s. It is limited by speed of device for reaching applied voltage. Thus, altering the measurement technique allows for increased registered current without changing the electrode materials or surface area.

Sensor calibration using the NPV and DPV techniques with a pulse time of 0.005 s (Figure S25, Supporting Information) and 0.1 s (Figure S26, Supporting Information) was performed to compare their performance with CA calibration at $t = 0.1$ s. It was found that at pulse width 0.005 s a strong current at -0.6 V (Figure S25a,b, Supporting Information) was observed even without hydroquinone although current at this voltage increased with concentration of hydroquinone. The reason of strong current at -0.6 V without hydroquinone is reduction of oxygen – reference experiments made on bare electrode without polymer brush and hydroquinone also show this current (Figure S24, Supporting Information). Due to the presence of this current and the lack of noise reduction due to the very short voltage pulses, the LOD and sensitivity obtained by NPV are 19 μM and 0.15 $\text{A} \cdot \text{M}^{-1}$, respectively (Table 2). The too noisy signal obtained by DPV didn't allow reliable determination of these parameters at all. Therefore, we focused on the pulse with 0.1 s when the charging current and current associated with reduction of oxygen are substantially lower than the faradaic current associated with the hydroquinone oxidation/reduction process.

Table 2. Sensor parameters obtained from calibration curves measured by different electrochemical techniques.

	Sensitivity, A·M ⁻¹	LOD, μM	Detection range*, μM
CA (at 2s)	0.12	2.2	7.3–115
CA (at 0.1s)	0.16	2.4	7.8–383
NPV (0.005 s)	0.15	19	63–238
NPV (0.1 s)	0.14	0.1	0.3–750
DPV (0.1 s)	0.068	0.08	0.2–350

*Upper limit of detection range was determined as $0.5 \times KV_m$, LOD was determined as $3 \cdot \sigma/S$, where σ – standard deviation of background current (empty buffer). The lower limit of the detection range was estimated as $LOQ = 10 \cdot \sigma/S$.

The results revealed that both methods (NPV and DPV) for pulse width 0.1 s (Figure 9) provide a significantly lower background current without a notable reduction in sensor sensitivity. The sensitivity values for NPV and DPV were 0.14 and 0.068 A·M⁻¹, respectively. The LOD decreased by more than an order of magnitude, reaching 0.096 and 0.075 μM for NPV and DPV, respectively. The lower limit of the detection range was estimated as the LOQ (10 times the standard deviation of the background current divided by sensitivity) and was found to be 0.3 and 0.2 μM for NPV and DPV, respectively. The upper limit of the detection range is difficult to determine precisely, as the plateau of the Michaelis–Menten fit was not reached. However, a careful estimation suggests that it is at least $\approx 0.5 \times K_m$, corresponding to ≈ 750 μM for NPV and 350 μM for DPV (Table 2).

When comparing the performance of our sensors with published enzymatic and nonenzymatic sensors for hydroquinone/quinone, we found that comparing them directionally is quite difficult because experiments were performed under different conditions, different activity of enzymes, scanning speeds, sample sizes, acquisition times for data averaging to reduce noise and not always all data are available for comparison. We considered the following parameters as criteria for benchmarking: sensitivity, LOD , and detection range. In many cases, the LOD was obtained by extrapolation, and the further the LOD value obtained from the lowest measured concentration (LMD), the less reliable it is. Therefore, we introduced the ratio between the lowest measured concentration (LMC) and the LOD , LMC/LOD , as a quality criterion for the results. Ideally, the LMC/LOD should

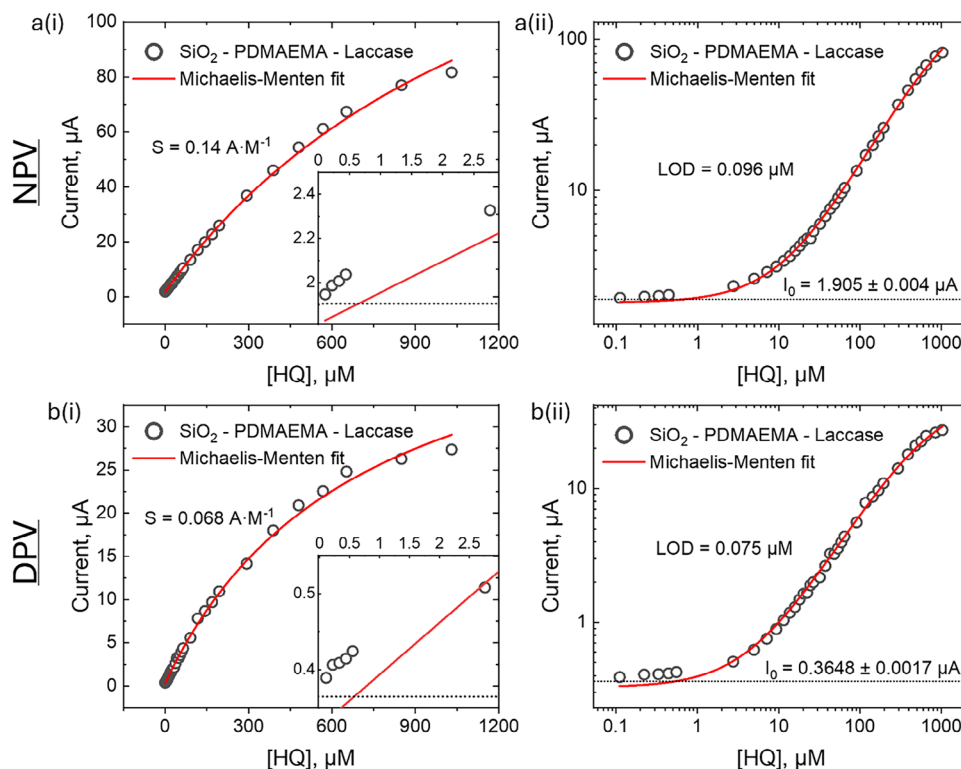


Figure 9. Calibration curves were obtained via (a) normal pulse voltammetry (NPV) and (b) differential pulse voltammetry (DPV) for HQ solutions of different concentrations in 0.1 M pH = 4 acetate buffer plotted in (i) lin-lin and (ii) log-log scale. The NPV was performed with 0.1 s pulse time, 1s sample period, and 10 mV step size. The DPV was performed with 0.1 s pulse time, 1s sample period, 10 mV step size, and 200 mV pulse. Dot – line shows the mean value of the blank buffer solution with its standard deviation.

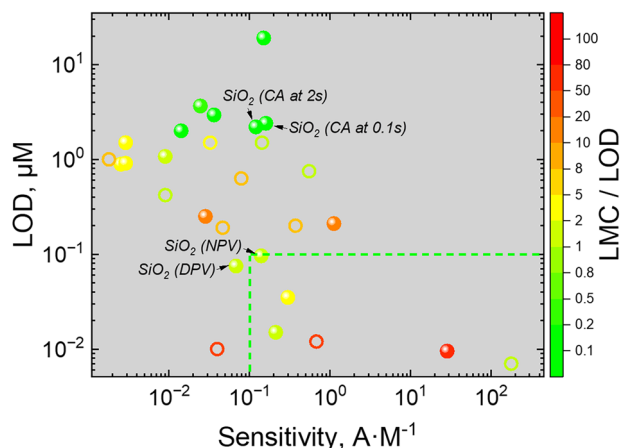


Figure 10. Ashby-like plot for LOD versus Sensitivity color-mapped by LMC/LOD ratio, where LMC is the lowest measured concentration. Full circles correspond to Laccase-based sensors; empty circles correspond to Laccase-free sensors. The points correspond to references in Supporting Information. For more information, please see the chapter “Comparison to other studies” in the Supporting Information.

be less than 1 so that a transition from the measured to the unmeasured range is observed. LMC/LOD greater than 20–50 is an indication that the LOD value is not highly reliable. Typically, determining LOD requires measuring the background current – the current without the analyte and its noise, which is not always measured. Actually, after selection and discarding enzyme-based biosensors with not reliably measured LOD , there is only one paper that demonstrate better results than ours is paper 2 (corresponds to the Supporting Information reference list). In this paper, the diameter of the electrode was 8 mm against 4 mm in our case that resulted in 4 times larger area and correspondingly 4 times larger current. Moreover, the activity of laccase used in this work ($23.3 \text{ U}\cdot\text{mg}^{-1}$) is nearly two orders of magnitude higher than the activity of laccase used in our work ($0.5 \text{ U}\cdot\text{mg}^{-1}$). Thus by plotting our results in an Ashby-like plot (Figure 10), we find that our sensor falls within the range of the most sensitive sensors, exhibiting one of the $LODs$ for hydroquinone detection. Enzyme-free sensors typically have higher sensitivity and lower LOD that is due to fast kinetics of reaction not limited by diffusion that allows high current. These sensors however issues with selectivity – enzyme-based biosensors allow selective detection. In any case, it is important that proper selection of measurement protocol allows substantial reducing LOD from more than $1 \mu\text{M}$ (for chronoamperometry) down to $\approx 0.1 \mu\text{M}$ (for NPV and DPV)

3. Conclusion and Outlook

In this work, we for the first time demonstrated the potential of nonconductive brush-decorated hairy carriers with physically adsorbed enzymes, in this case *Laccase*, for hydroquinone detection and showed principal ability of such systems for enzyme storage and use for bioelectrocatalysis. Our approach offers several advantages: i) Controllable high enzyme immobilization density: *Laccase* immobilized on PDMAEMA brushes reaches the enzyme content up to $0.57 \text{ g}\cdot\text{g}^{-1}$ of polymer and provides an environment where enzyme activity is 75 times higher compared to the ini-

tial buffer solution. ii) Efficient bioelectrocatalysis at the electrode surface: High amount and activity of enzymes reveal ineffective oxidation of HQ and distinct catalytic shape of CV curve. The *Laccase* oxidizes HQ fast and efficiently creating higher efficient quinone concentration near the electrode than that of HQ in bulk by enabling multiple oxidation/reduction cycles between enzyme and electrode surface. In other words, enzyme allows amplification of current signal that increases sensitivity compared to electrodes without enzyme. iii) Increased sensitivity and lower detection limit: regardless of the nonconductive nature of the carrier, the sensor is able to demonstrate high sensitivity (up to $0.16 \text{ A}\cdot\text{M}^{-1}$) the ability to efficiently detect hydroquinone over a large concentration range ($0.2 - 750 \mu\text{M}$). Moreover, the limitation of enzymes' catalytic activity was not reached due to their abundance and the upper detection limit can be increased even further by introducing mass transfer. The reliability of the literature data was evaluated by introducing the LMC/LOD ratio, which shows how accurately the LOD was determined. Among the reliable literature data, the sensor showed the best performance among the *Laccase*-based aerometric sensors.

The charge-stabilized principle of enzyme immobilization offers significant room for improvement. The signal can be amplified by varying the brush thickness, which affects the amount of immobilized enzymes. Additionally, enhancing charge transfer through the use of conductive carriers may increase enzyme affinity for substrates, enabling the detection of even lower substrate concentrations. It is also important to consider that the type of enzyme affects its substrate affinity to it. Therefore, different sources of laccase can result in varying sensor performance. Furthermore, the use of PDMAEMA brushes is not limited to laccase; other enzymes can also be immobilized for bioelectrocatalytic applications.

4. Experimental Section

Chemicals: Tetraethyl orthosilicate (TEOS, Sigma, 99%), ammonia solution (NH_4OH , Sigma, 28–30% solution), ethanol abs. (EtOH, Sigma, 99.9%), copper(II) bromide (CuBr_2 , Sigma, 99.999%), (3-aminopropyl)triethoxysilane (APTES, Sigma, 99%), α -bromoisobutryl bromide (Sigma, 98%), propionyl bromide (Sigma, 97%), tris(2-pyridylmethyl)amine (TPMA, Sigma, 98%), tin(II) 2-ethylhexanoate (Sigma, 95%), ethyl α -bromoisobutyrate (EBiB, Sigma, 98%), Laccase from *Trametes Versicolor* (Sigma, $\geq 0.5 \text{ U}\cdot\text{mg}^{-1}$), 2,2'-azino-bis(3-ethylbenzthiazoline-6-sulphonic acid) diammonium salt (ABTS, Sigma, $\geq 98\%$), N,N-Dimethylformamide (DMF, anhydrous, Sigma, 99.8%), Dichloromethane (DCM, Extra Dry, Thermoscientific, 99.8%), and Triethylamine (Et_3N , Sigma, $\geq 99.5\%$), hydroquinone (HQ, Sigma, 99%), potassium hexacyanoferrate (III) ($\text{K}_3[\text{Fe}(\text{CN})_6]$, Sigma, 99.98%), potassium chloride (KCl, Sigma, 99.0–100.5%), sodium acetate (CH_3COONa , Sigma, $\geq 99\%$), acetic acid (CH_3COOH , Sigma, $\geq 99.7\%$) were used as received. 2-(Dimethylamino)ethylmethacrylate (DMAEMA, Sigma, 98%), sodium azide (NaN_3 , Sigma, $\geq 99.5\%$) was passed through basic, neutral and acidic aluminum oxide columns for 20 min to remove the inhibitor, prior to polymerization.

Synthesis of Native SiO_2 Particles and Surface Modification: 200 nm SiO_2 particles were synthesized using the Stöber method.^[16] In the first step, a seed solution was prepared by mixing 50 mL of ethanol and 3 mL of NH_4OH (28–30%) in a clean 500 mL snap-top bottle at 500 rpm for 3–4 min. After stirring at room temperature for 12 h, 50 mL of the resulting mother solution (100 nm SiO_2 particles) was transferred to a new vial and 350 mL of ethanol and 24 mL of NH_4OH (28–30%) were added. After stirring for 3–4 min, 12 mL of tetraethyl orthosilicate (TEOS) was

added dropwise. After stirring at room temperature for 12 h, the resulting 200 nm SiO₂ particles were separated by centrifugation at 12 000 rpm for 10 min, washed five times with ethanol, and dried under vacuum at 60 °C overnight.

The particle surface modification was also carried out in two steps. First, APTES modification was performed and then the bromine-containing functional groups were modified. First, SiO₂ particles (2 g) were placed in a 250 mL round-bottom flask with a stirring bar, and 95 mL of ethanol and 5 mL of 3-aminopropyltriethoxysilane (APTES, Sigma, 99%) were added. After stirring at room temperature for 12 h, the particles were separated by centrifugation at 12 000 rpm for 10 min, washed with ethanol 5 times, and vacuum dried at 60 °C overnight. Second, 1 g of APTES-modified SiO₂ particles were added to a 100 mL round-bottom flask with a stirring bar, 50 mL of dichloromethane, stirred for 3 min, then 0.5 mL of α -bromoisobutryl bromide (Br-Initiator, Aldrich, 98%) and 0.36 mL of propionyl bromide (Aldrich, 97%), stir for 3 min, add 2 mL of triethylamine, stir the resulting solution at 700 rpm at room temperature, centrifuge at 12 000 rpm for 10 min after 2 h to collect the particles, wash twice with DCM, wash three times with ethanol, and dry overnight at 60 °C in a vacuum.

Synthesis of Core-Shell SiO₂-PDMAEMA Particles: 500 mg of BrIn-premodified silica particles were placed in a test tube with a ground glass joint, septum and stir bar and monomer, solvent, 30 μ L CuBr₂ (0.1 M in DMF), the 6.5 mg ligand and 0.15 μ L ethyl- α -bromoisobutyrate (EBIB) were added while stirring. The dispersion was rinsed with argon in an ultrasonic bath. After 10 min, the appropriate reducing agent was added. The reaction was carried out in a water or oil bath at the appropriate temperature and time and at 800 rpm while stirring. The particles were separated by centrifugation and the supernatant was saved for Gel Permeative Chromatography (GPC). The particles were washed several times in EtOH and dried at 25 °C in a vacuum.

Immobilization of Laccase and Activity Measurements: 10 mg of polymer-modified SiO₂ particles were washed thrice with buffer solution (10 mM sodium acetate, pH 4) and dispersed in 500 μ L buffer. 500 μ L of enzyme solution (\approx 32 U mL⁻¹) in sodium acetate buffer was added and immobilized at room temperature for 1 h under gentle shaking. This was followed by collecting the supernatant and washing the particles with sodium acetate buffer using centrifugation until no enzyme activity was measured in the supernatant. Afterward, the activity of immobilized particles was measured using ABTS activity assay.

Tristar5 multifunctional microplate reader (Berthold Technologies) was used to measure the Laccase activity using ABTS assay at 25 °C. Laccase oxidizes the substrate 2,2'-azino-bis(3-ethylbenzthiazoline-6-sulphonic acid) (ABTS) to cation radical ABTS⁺ with a color change from colorless to green, which was measured by UV/Vis spectroscopy at 420 nm. The activity of the enzyme was calculated by the absorbance change (ΔE) per time interval (Δt) divided by the extinction coefficient of the ABTS at 420 nm (ϵ_{ABTS} , 36000 M⁻¹ cm⁻¹) times the path length (d) Equation (3).

$$\text{Activity} = \frac{\Delta E}{\epsilon \cdot d \cdot \Delta t} \quad (3)$$

The enzyme activity on a particle or polymer was calculated using Equation (4).

$$\text{Activity} \left(\frac{U}{\text{mg particle or polymer}} \right) = \frac{\text{Activity of immobilized enzyme}}{\text{mass of particle or polymer}} \quad (4)$$

The enzyme immobilization yield was determined by calculating the ratio of the activity of the immobilized enzyme on particles and the activity of the free enzyme before immobilization Equation (5):

$$\begin{aligned} &\text{Enzyme immobilization yield} \\ &= \frac{\text{Activity of immobilized enzyme on particles}}{\text{Initial activity of free enzyme before immobilization}} \quad (5) \end{aligned}$$

Modification of Working Electrode and Electrochemical Assays: The commercial 4 mm graphite screen-printed electrodes (BVT Technologies) were modified by drop-casting of 10 μ L with a concentration of 10 mg mL⁻¹ particles suspension in 0.1 M pH = 4 acetate buffer onto working electrode followed (3 mm diameter) by drying on air. After drying, the modified electrodes were left in the acetate buffer overnight at 4 °C. Prior measurements, the electrodes were cleaned by 50 times cycling of electrodes in -0.8–0.8 V range at 100 mV s⁻¹ in pure acetate buffer to ensure that there were no contaminating signals. All electrochemical measurements were performed on Gamry 1010E potentiostat.

For further investigation of charge transport the heterogeneous rate constant k_0 was evaluated, using the following Equation (6):

$$k_0 = \frac{RT}{n^2 F^2 A R_{ct} C} \quad (6)$$

where n – number of electrons transferred during redox process, A – active surface area (cm²), R_{ct} – charge transfer resistance obtained from EIS data, C – concentration of electroactive species (mol·cm⁻³), R – ideal gas constant (8.314 J·mol⁻¹·K⁻¹), T – temperature. F – Faraday constant (96485 C·mol⁻¹). The active surface area A was calculated, using Randles-Sevcik Equation (7):

$$i_p = 0.446 n F A C \left(\frac{n F \nu D}{RT} \right)^{\frac{1}{2}} \quad (7)$$

where i_p – is reduction peak, A – electroactive surface area of electrode, C – bulk analyte concentration, ν – scan rate, F – Faraday constant, D – diffusion coefficient, T – Temperature.

Thermogravimetry: The thermogravimetry was performed on TG 209 F3 Tarsus, Netzsch at a heating rate of 10 K min⁻¹ in a nitrogen atmosphere. The polymer brush thickness t was calculated according to Equation (8):

$$t = \frac{R * \rho_{SiO_2} * \varphi_{Polymer}}{3 * \rho_{polymer} * (1 - \varphi_{Polymer})} \quad (8)$$

where R – silica particles radius, $\rho_{(SiO_2)}$ – silica density (2.4 g cm⁻³), φ – PDMAEMA mass fraction, $\rho_{polymer}$ – PDMAEMA density (1.318 g cm⁻³).

Gel Permeative Chromatography: The number average molecular mass, M_n , and weight average molecular weight, M_w , and polydispersity index, PDI (PDI = M_w / M_n), were determined by GPC (Agilent 1260 Infinity). The measurements were carried out at 60 °C. The eluent for GPC measurements was DMF of high-performance liquid chromatography grade with the addition of 0.01 M LiBr, and the standards used for calibration were monodisperse poly(methyl methacrylate).

Supporting Information

Supporting Information is available from the Wiley Online Library or from the author.

Acknowledgements

The authors acknowledge the project funding from DFG (Grants SY125/15-1 and IO 68 20–1).

Conflict of Interest

The authors declare no conflict of interest.

Author Contributions

The manuscript was written through contributions of all authors. All authors have given approval to the final version of the manuscript.

Data Availability Statement

The data that support the findings of this study are available in the supplementary material of this article.

Keywords

bioelectrocatalysis, electrochemical biosensor, hairy core-shell particles, laccase, polymer brush

Received: March 25, 2025

Revised: May 7, 2025

Published online:

- [1] a) S. Palanisamy, S. K. Ramaraj, S.-M. Chen, T. C. K. Yang, P. Yi-Fan, T.-W. Chen, V. Velusamy, S. Selvam, *Sci. Rep.* **2017**, *7*, 41214; b) V. A. Arlyapov, S. S. Kamanin, O. A. Kamanina, A. N. Reshetilov, *Nanotechnol. Russ.* **2017**, *12*, 658; c) Y. Liu, X. Nan, W. Shi, X. Liu, Z. He, Y. Sun, D. Ge, *RSC Adv.* **2019**, *9*, 16439.
- [2] a) M. D. Alvau, S. Tartaggia, A. Meneghello, B. Casetta, G. Calia, P. A. Serra, F. Polo, G. Toffoli, *Anal. Chem.* **2018**, *90*, 6012; b) C. Rinaldi, D. K. Corrigan, L. Dennany, R. F. Jarrett, A. Lake, M. J. Baker, *ACS Sens.* **2021**, *6*, 3262.
- [3] S. Gavrilaş, C. Ş. Ursachi, S. Perța-Crișan, F.-D. Munteanu, *Sensors* **2022**, *22*, 1513.
- [4] Y. Bai, D. Zhang, Q. Guo, J. Xiao, M. Zheng, J. Yang, *ACS Biomater. Sci. Eng.* **2021**, *7*, 787.
- [5] M. E. Peterson, R. M. Daniel, M. J. Danson, R. Eisenthal, *Biochem. J.* **2007**, *402*, 331.
- [6] a) P. N. Durán, M. A. Rosa, A. D'Annibale, L. Gianfreda, *Enzyme Microb. Technol.* **2002**, *31*, 907; b) M. Iqhrammullah, A. Fahrina, W. Chiari, K. Ahmad, F. Fitriani, N. Suriaini, E. Safitri, K. Puspita, *Macromol. Chem. Phys.* **2023**, *224*, 2200461.
- [7] a) L. Yang, X. Peng, S. Zhang, G. Xie, X. Zhang, *J. Mater. Sci.* **2023**, *58*, 6839; b) S. Sharma, R. Sahney, P. Dahiya, *Polym. Bull.* **2024**, *81*, 3973; c) I. Sulym, J. Zdarta, F. Ciesielczyk, D. Sternik, A. Derylo-Marczewska, T. Jesionowski, *Materials* **2021**, *14*, 2874. d) N. R. Mohamad, N. H. C. Marzuki, N. A. Buang, F. Huyop, R. A. Wahab, *Biotechnol. Biotechnol. Equip.* **2015**, *29*, 205; e) Y. R. Maghraby, R. M. El-Shabasy, A. H. Ibrahim, H. M. E.-S. Azzazy, *ACS Omega* **2023**, *8*, 5184.
- [8] H. Chen, O. Simoska, K. Lim, M. Grattieri, M. Yuan, F. Dong, Y. S. Lee, K. Beaver, S. Weliwatte, E. M. Gaffney, S. D. Minteer, *Chem. Rev.* **2020**, *120*, 12903.
- [9] I. Bravo, M. Prata, A. Torrinha, C. Delerue-Matos, E. Lorenzo, S. Morais, *Bioelectrochemistry* **2022**, *144*, 108033.
- [10] Y. Zhang, X. Li, D. Li, Q. Wei, *Colloids Surf., B* **2020**, *186*, 110683.
- [11] M. Chandran, E. Aswathy, I. Shamna, M. Vinoba, R. Kottappara, M. Bhagiyalakshmi, *Mater. Today: Proc.* **2021**, *46*, 3136.
- [12] O. Kudina, A. Zakharchenko, O. Trotsenko, A. Tokarev, L. Ionov, G. Stoychev, N. Pureskiy, S. W. Pryor, A. Voronov, S. Minko, *Angew. Chem., Int. Ed.* **2014**, *53*, 483.
- [13] J. Bebić, K. Banjanac, M. Čorović, A. Milivojević, M. Simović, A. Marinković, D. Bezbradica, *Chin. J. Chem. Eng.* **2020**, *28*, 1136.
- [14] C. Marschelke, I. Raguzin, A. Matura, A. Fery, A. Synytska, *Soft Matter* **2017**, *13*, 1074.
- [15] Y. Zhao, Y. Zheng, R. Kong, L. Xia, F. Qu, *Biosens. Bioelectron.* **2016**, *75*, 383.
- [16] W. Stöber, A. Fink, E. Bohn, *J. Colloid Interface Sci.* **1968**, *26*, 62.
- [17] B. A. Kuznetsov, G. P. Shumakovich, O. V. Koroleva, A. I. Yaropolov, *Biosens. Bioelectron.* **2001**, *16*, 73.
- [18] a) M. M. Rodríguez-Delgado, G. S. Alemán-Nava, J. M. Rodríguez-Delgado, G. Dieck-Assad, S. O. Martínez-Chapa, D. Barceló, R. Parra, *TrAC, Trends Anal. Chem.* **2015**, *74*, 21; b) B. Haghghi, L. Gorton, T. Ruzgas, L. J. Jönsson, *Anal. Chim. Acta* **2003**, *487*, 3.